25

High Resolution Far Infrared Spectra of the Semiconductor Alloys Obtained Using the Synchrotron Radiation as Source

E.M. Sheregii
University of Rzeszow, Rzeszów
Poland

1. Introduction

It is known that far-infrared (FIR) spectra give direct information on phonon modes and impurity levels in the crystal lattices. Infrared spectroscopy enable us also to obtain information about real crystalline microstructure and interior interactions of the semiconductor solid solutions (Barker & Sievers, 1975; Robouch et al.,2001).

A role of the semiconductor alloys in electronics and optoelectronics increases constantly. Since the electron-phonon interaction is main mechanism of the current carriers scattering in semiconductors it is important to recognize deeply the phonon spectra of the semiconductors solid solutions. The results on the semiconductor alloy FIR-spectra collected during 70, 80 and 90 decades have not been explained satisfactorily on base of simple "two-mode behavior" for ternary and "three-mode behavior" for quaternary alloys. The previous reviews and books dedicated to the phonon spectra of semiconductor's compounds (Barker & Sievers, 1975;Tylor,1988;Adachi,1999;Kosevich,1999) give not a reasonable answers on the questions concerning: whether the vibrations of different dipole pairs in the solid solution are connected in the alloy lattice and form a running wave (phonons) or on the contrary: they are disseminated on great number of local modes? Another one concerning of the solid solutions microstructure – geometry of chaos: whether this geometry factor is sufficient or thermodynamic one is necessary to add. The adequate describing of this geometry factor applying to the phonon spectra interpretation should be developed both for ternary alloys and quaternary also.

In order to give answers on these principally important question we need the credible experimental results and for this purpose in years 2001-2006 were performed in Laboratory Nationale di Frascati the six TARI (Transnational Access to the Research Infrastructure) Projects concerning the FIR-spectra of the semiconductor solid solutions obtained by measuring of optical reflectivity using synchrotron radiation as source. The brilliant properties of synchrotron radiation enable us to obtain FIR-spectra of comparably high resolution: about 1 cm^{-1} whereas nature sources provided 2.5 cm^{-1} at better case. The results on FIR-spectra obtained by this way for mercury contained semiconductor alloys – ternary as $Hg_{1-x}Cd_xTe$ as well as quaternary like $Zn_yCd_xHg_{1-x-y}Te$ – will be presented in this Chapter. There is third principally important question concerning Hg-contained solid solutions:

additional lines arousing constantly in the region of frequencies lower then main HgTe-like modes. The cause of appearing of these additional lines was not explained (Baars & Sorgers, 1972;)Amirtharaj et al, 1990;Biao,1996;Rath et al., 1995). The new results as well as previous published ones (Sheregii et al, 2006; Cebulski, et al.,2008;Polit et al., 2010;Sheregii et al.,2009;Sheregii et al.,20011) but with new interpretation, will be presented here and allow us partly to respond on the formulated above questions.

2. Experiment

2.1 Experimental technique

The optical reflection spectra in the region from 10 to 10 000 cm^{-1} where the phonon frequency values (30 – 400 cm^{-1}) of semiconductor's compounds are located, were measured in the wide temperature interval and composition region. Experiments were performed at the DAFNE-light laboratory at Frascati (Italy) using the experimental set-up described in (Cesteli Guidi et al., 2005). A BRUKER Equinox 55 FT-IR interferometer modified to collect spectra in vacuum and both the synchrotron radiation light emitted by the DAFNE storage ring as well as a mercury lamp were used as IR sources (Marcelli et al., 2005). The measurements were performed in the temperature range of 20-300 *K* at the spectral resolution of 1 cm^{-1} (2 cm^{-1} in some cases) collecting typically 200 scans within 600 s of acquisition time with a bolometer cooled down to 4.2 *K*.

The reflectivity was measured by using as a reference a gold film evaporated onto the surface of the investigated samples. This method enabled us to measure the reflectivity coefficient with an accuracy of about 0.2 %. The imaginary part curves of the dielectric function $Im[\varepsilon(\omega,T)]$ were calculated, from reflectivity spectrum, by means of the Kramers-Kronig (KK) procedure with uncertainty less than 1.5%.

2.2 Experimental results for ternary alloys

In the our previous published works were presented results obtained by the same way on the ternary solid solutions $Hg_{1-x}Cd_xTe$ and $Hg_{1-x}Zn_xTe$ (Cebulski, et al.,2008;Polit et al., 2010;Sheregii et al.,2009;Sheregii et al., 2011). It was shown in these works that observed subtle structure of the two phonon sub-bands in case of ternary alloys can be successfully explained on base of the five structural cells model of H.W.Verleur and A.S. Barker (V-B model) (Verleur & Barker, 1966) thought the additional phonon lines were observed. Last one required the new hypothesis – the two wells potential model for Hg-atoms in lattice (Polit et al., 2010) – for explanation the experimental spectra. The V-B model will be presented in next sub-chapter. In this sub-chapter are exposed the FIR-spectra concerning ternary alloys in order to illustrate the fact of multi-mode behaviour – main statement of the random version of the V-B model which is necessary to interpret of the experimental FIR-spectra.

The high-resolution reflection FIR-spectra obtained for the ternary $Hg_{1-x}Cd_xTe$ for compositions from x=0.06 to x=0.7 at the temperature 300K and in the spectral range 100 cm^{-1} to 200 cm^{-1} are shown in Fig.1 as reflectivity curves $R(\omega)$. Two bands which shift weakly with the composition are observed: first one around 118-128 cm^{-1} and second one around 145-155 cm^{-1}. The amplitude of first band increases when the content of *HgTe* increases and amplitude of second band increases when the *CdTe* content increases. The first band

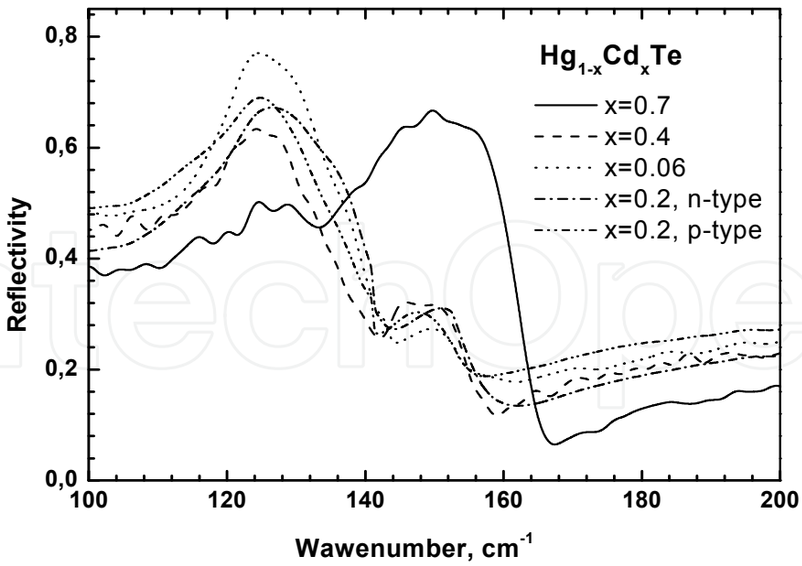

Fig. 1. Reflectivity spectra $Cd_xHg_{1-x}Te$ (x is changing from 0.06 to 0.7) obtained at 300K.

corresponds to the *HgTe*-like sub-band and second one – to the *CdTe*-like sub-band.. This type of reflectance spectrum again shows according to previous work (Baars & Sorgers, 1972; Amirtharaj et al.,1990; Biao,1996; Rath et al., 1995) two-mode behavior of the optical phonons in the $Hg_{1-x}Cd_xTe$ alloys. Whereas, the subtle structure of both sub-bands is clearly observed too what undoubtedly indicates on multi-mode character of phonon spectra (above two modes). Authors (Kozyrev et al.,1998) interpreted these subtle structure in frame of the V-B model but they limited consideration of the FIR-spectra in the spectral region 118 – 160 cm^{-1} . Whereas, in the region 90 – 116 cm^{-1} are observed additional lines registered earlier (Talwar, 1984; Amirtharaj et al., 1990;Biao,1996;Rath 1995). The line amplitudes of main sub-bands (HgTe-like at 118 – 130 cm^{-1} as well as CdTe-like at 140 – 170 cm^{-1}) decrease when the temperature increases for both samples. Contrary, the line amplitudes of additional lines (we can call them as Additional Phonon Modes (APM) whereas the main sub-bands we can called as Canonical Phonon Modes (CPM)) increase when the temperature increases. That is clearly shown on the temperature dependence of FIR-spectra presented in Fig. 2 and 3.

In Fig.2 are shown the FIR-spectra as reflectivity curves $R(\omega)$ for the n-type $Hg_{0.8}Cd_{0.2}Te$ alloy in the temperature region 30 K – 300 K. The temperature dependence of reflectivity curves $R(\omega)$ for p- $Hg_{0.8}Cd_{0.2}Te$ alloy is presented in Fig. 3. We may see the shift of the *HgTe-like* band towards the higher frequency side with increase of the temperature and shift of the *CdTe-like* band to the lower frequency side when the temperature increases similarly to results obtained in (Roth et al.,1995). The main *TO* – phonon mode frequency of *HgTe* -like sub-band increases from 118 cm^{-1} at 30K to 121 cm^{-1} at 300 K for n-type alloy. We have inferred from the FIR-spectra that the sings of the temperature induced shifts of the *HgTe* – like and *CdTe* –like mode frequencies in the MCT alloy are opposite to each other for the composition range $x \leq 0.3$. The *CdTe* –like mode frequency decrease from 154.2 cm^{-1} to 152 cm^{-2} with the increase in temperature from 30K to 300K and the intensity of the *HgTe*-like and *CdTe*-like *TO* mode decreases and higher background is observed for the *p*-type $Hg_{0.8}Cd_{0.2}Te$ in the spectral range 90 cm^{-1}- 115 cm^{-1}.

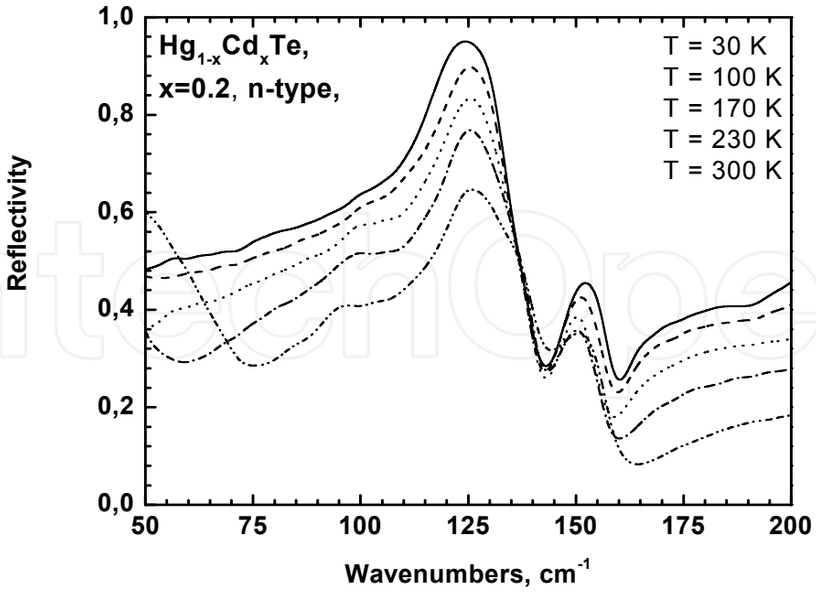

Fig. 2. Reflectivity spectra of n- $Cd_{0.2}Hg_{0.8}Te$ in the temperature range 30 K – 300 K.

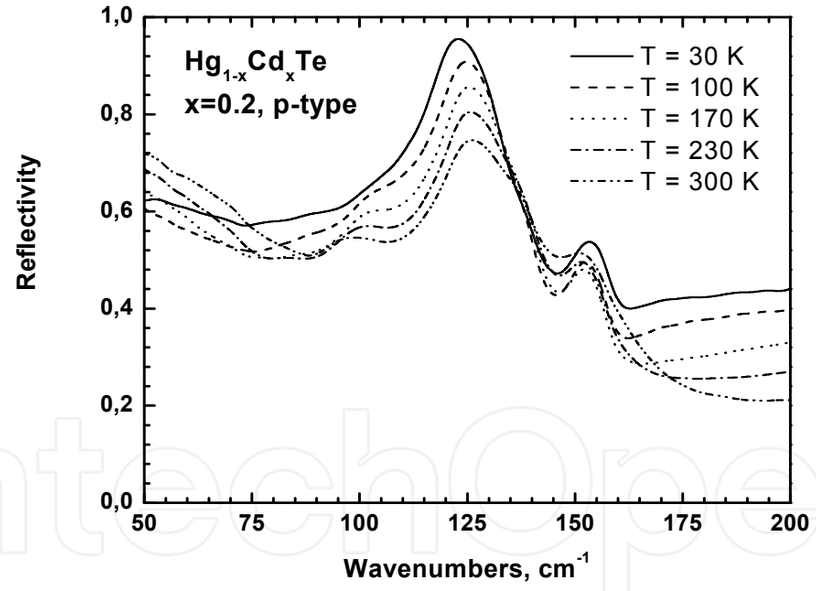

Fig. 3. Reflectivity spectra of p- $Cd_{0.2}Hg_{0.8}Te$ in the temperature range 30 K – 300 K.

In case of p-type $Cd_{0.2}Hg_{0.8}Te$ alloy the main *TO* – phonon mode frequency of *HgTe* -like sub-band increases from 118 cm^{-1} at 30K to approximately 122 cm^{-1} at 300 K.

2.3 Experimental results for quaternary alloys

The introduction of low amounts of Zn stabilizes the weak Hg–Te bonds, in crystal lattice of the MCT solid solution, while Cd destabilizes them (Sher et al.,1985). The introduction of a third metal cation (Zn for example), by substitution of matrix cations (Hg or Cd) in solid

solution lattices with a common anion ($Zn_xCd_yHg_{1-x-y}Te$ or ZMCT in our case), enables us to control the material parameters with one extra degree of freedom (Cebulski et al., 1998). The bulk quaternary layers of $Zn_xCd_yHg_{1-x-y}Te$ were obtained by liquid phase epitaxial technique on the CdTe substrates in A.F. Joffe Physical-Technical Institute (St.Petersbourg, Russion), the compositions of samples are shown in Table 1. The thickness of the homogeneous layer was 4 μm. The surface of samples was natural (110) plane of grown layer and was ideal for optical measurements.

Number of sample	x, mol %	y, mol.%
I	0.020	0.200
II	0.070	0.21
III	0.120	0.17
IV	0.127	0.117
V	0.180	0.120
VI	0.050	0.230
VII	0.120	0.130

Table 1. Compositions of the $Zn_xCd_yHg_{1-x-y}Te$ samples investigated.

Optical reflectivity from surface of nine $Zn_xCd_yHg_{1-x-y}Te$ samples of seven compositions in the far-infrared region was measured using the synchrotron radiation as source (high resolution FIR-spectra – the reflectivity experiment is described above)). Some of results were published earlier (Sheregii et. al., 2006). The measurements of reflectivity were performed in temperature region from 30 K to 300 K. In Fig. 4 and 5 are presented reflectivity FIR-spectra obtained for two compositions of $Zn_xCd_yHg_{1-x-y}Te$ for three temperatures: 30 K, 100K and 300 K.

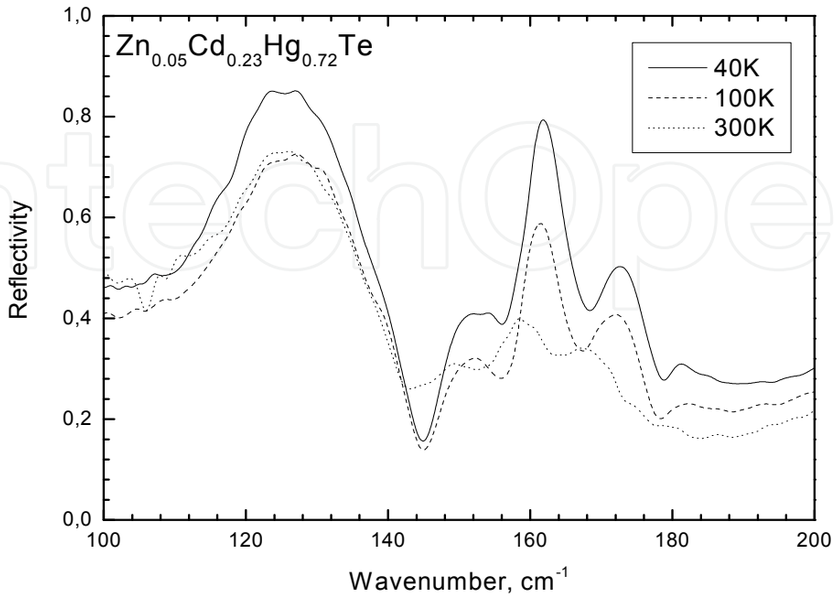

Fig. 4. Reflectivity Spectra of $Zn_{0,05}Cd_{0,23}Hg_{0,72}Te$ (sample VI).

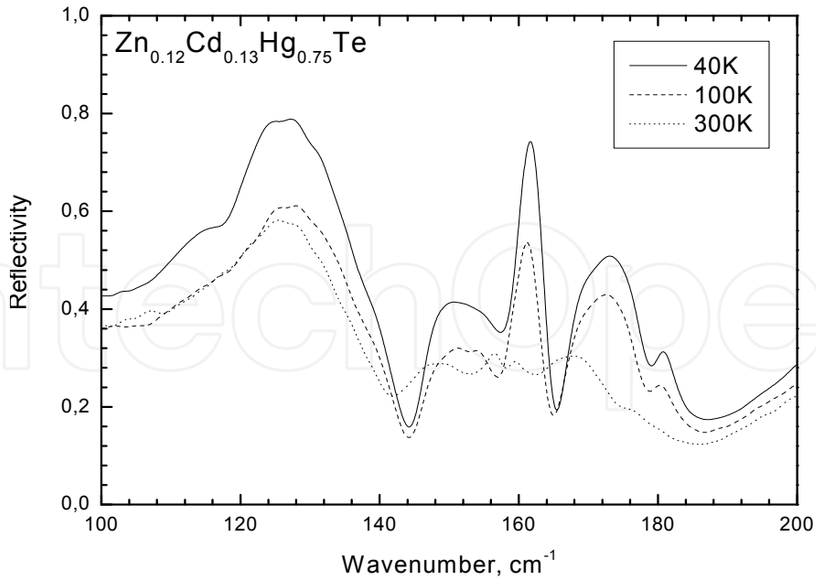

Fig. 5. Reflectivity Spectra of $Zn_{0,12}Cd_{0,13}Hg_{0,75}Te$ (sample VII).

These curves are similar to typical reflection spectra but these curves have a much richer structure of spectra, as were observed for ternary alloys. It is seen three main bands at 130 cm^{-1}, 160 cm^{-1} and 180 cm^{-1} can be point out in the reflective spectra. However, each of these sub-bands has additional subtle structures, which point to the superposition of a greater number of lines. With increasing of temperature from 30 K to 300 K the subtle structure of observed sub-bands became more smooth.

3. Discussion

3.1 Spectral analyses of the ternary alloy FIR-spectra

The lines corresponding to phonon modes are clearly observed on the *Im[ε(ω)]* curves calculated by Kramers-Kroning analyses from the experimental FIR reflectivity curves *R(ω)*. In Fig.6 and 7 are shown *Im[ε(ω)]*–curves for *p*-$Hg_{0.8}Cd_{0.2}Te$ obtained for temperature 300 K and 30 K, respectively. In Fig. 6 we can see considerable asymmetry of HgTe-bands caused by additional lines in the range of 90 cm^{-1} –115 cm^{-1}. That are the additional lines origin of which is discussed during last two decades. The dispersion analysis of the CPMs and APMs was performed by approximating the *Im[ε(ω,T)]* curves by the Lorentzian sum

$$\mathrm{Im}\,\varepsilon(\omega) = \sum_{i=1}^{k} \frac{S_i \gamma_i \omega}{(\omega_{TOi}^2 - \omega^2)^2 + \omega^2 \gamma_i^2} \tag{1}$$

where S_i, ω_{TOi} and γ_i are the oscillator strength, frequency and damping parameters of the *i*-phonon mode, respectively. The results of spectral analysis for *p-Hg0.8Cd0.2Te* are presented in Fig.6 and for *n-Hg0.8Cd0.2Te in Fig.* 7. Parameters of Lorentzian's oscillators used for fitting the *Im[ε(ω,T)]*-curves are shown in Table 2.

In Table 3 the oscillator strengths sum for APM are shown separately as $(\Sigma S_{HgTe})_{add}$. There are nine well-resolved oscillators for *p*-type *Hg0.8Cd0.2Te* at 30 *K* and eleven for this sample at

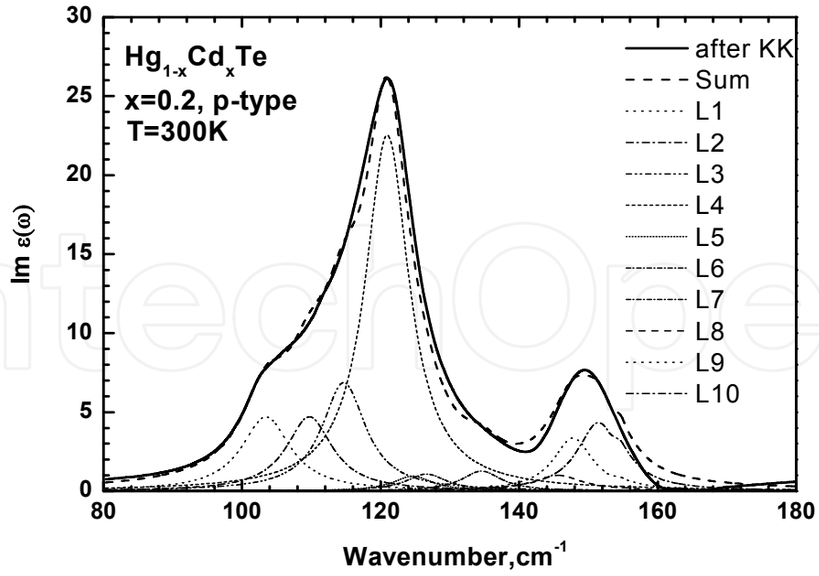

Fig. 6. Imaginary part of the dielectric function od $Hg_{0,8}Cd_{0,2}Te$ *p*- type in the temperature 300K.

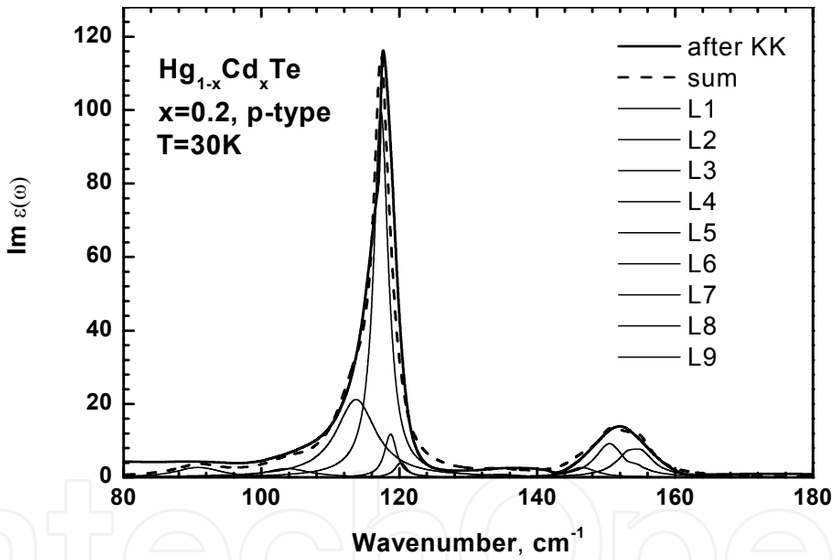

Fig. 7. Imaginary part of the dielectric function of $Hg_{0,8}Cd_{0,2}Te$ *p*- type in the temperature 30K.

300 *K*. The position of main *HgTe*-line for *p*-type is 118 cm^{-1} at 30 *K* and is the same as for *n*-type sample while the oscillator strengths of these lines for n- and p-type samples are drastically different: 62500 cm^{-2} for *n*-type and 39000 cm^{-2} for *p*-type, respectively. The damping factor is nearly two times larger for *p*-type $Hg_{0,8}\ Cd_{0,2}\ Te$ because the line shape is much asymmetric and wider in comparison with the *n*-type $Hg_{0,8}\ Cd_{0,2}\ Te$.

It is interesting to consider in details the temperature behavior of the observed phonon modes for both *n*- and *p*-type $Hg_{0.8}Cd_{0.2}Te$. In Figures 8 and 9 are shown the temperature dependences of frequencies for observed phonon lines of the *HgTe*-like and *CdTe*-like sub-bands (CPMs) of *n*- and *p*-type samples. It is seen that only one *HgTe*-like mode is observed at 30K and two *CdTe*-like mode for *n*- $Hg_{0.8}Cd_{0.2}Te$ (see Fig.7).

Temperature [K]	Number of Line	S	ω	γ	$\sum S_{HgTe}$		$\sum S_{CdTe}$	
					CPM	AVM	CPM	AVM
30	1	600	91,00	5.0		6200		
	2	1500	107.0	4.0				
	3	4700	112.4	4.0				
	4	48000	118.0	3.5	48000			
	5	500	135.0	7.0				500
	6	1300	148.0	5.0			15800	
	7	5800	151.0	5.0				
	8	8700	154.2	6.2				
300	1	4200	103.7	8.6		11400		
	2	4200	110.0	8.1				
	3	6100	115.0	7.7				
	4	21100	121.3	7.7	31300			
	5	830	125.0	7.0				
	6	1000	127.0	7.0				
	8	1200	135.0	7.0				1000
	9	1300	146.1	8.9			9690	
	10	3500	148.3	7.0				
	11	4890	152.0	7.4				

Table 2. Parameters of Lorentzian's oscillators used for fitting the *Im[ε(ω,T)]* –curves of the *p- $Hg_{0.8}Cd_{0.2}Te$* for the temperatures 30 K and 300K.

Temperature [K]	$s^i_{HgTe} = \frac{S^i_{HgTe}}{\omega^2}$	$\left(\sum_j s^j_{HgTe}\right)_{add}$
30	2.8	0.5
300	1.54	1.19

Table 3. The oscillator's sums of the CPM and AVM for *p- $Hg_{0.8}Cd_{0.2}Te$* at 30 K and 300K.

When the temperature is higher than 100K the splitting on two *HgTe*-like modes takes place and at last at 300 *K* the three *HgTe*-like CPMs are displayed in case of *n*-type sample. Whereas in the region 90 – 115 cm^{-1}, one weak line is observed at 108 cm^{-1} which amplitude increases with increasing of temperature and after 230 *K* this line is splitted on three ones in the range 106 – 118 cm^{-1}.

We can see a considerably larger number of lines for p-type sample in comparison with *n*-type sample but the temperature shift of the phonon mode frequencies is similar. These results obtained for the *n*- and *p-$Hg_{0.8}Cd_{0.2}Te$* at 30 *K* agree generally with data presented in (Rath et al., 1995) but in this work was not performed a comparison for *n*- and *p*-type

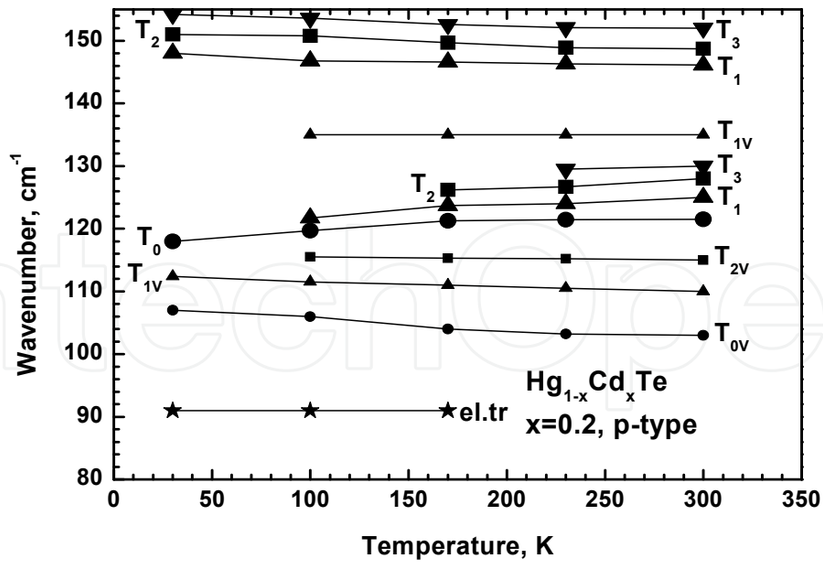

Fig. 8. The temperature dependencies of the phonon mode frequencies for the *p*- type The $Hg_{0.8}Cd_{0.2}Te$, shown in Fig. 2 and 3 as well as in Table II and III. T_0, T_1 and T_2 are tetrahedra generated the corresponding CPM modes. The T_{nv} are tetrahedra generated by the corresponding APM modes.

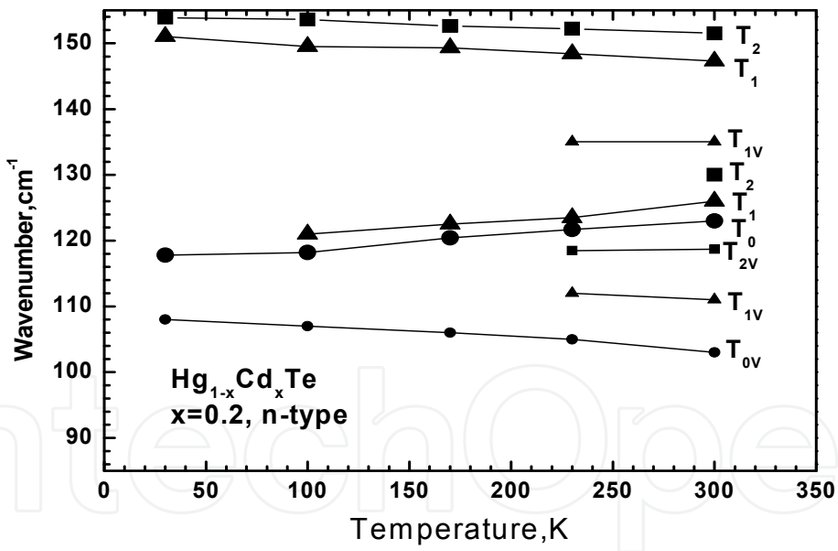

Fig. 9. The temperature dependencies of the phonon mode frequencies for the *n*- type $Hg_{0.8}Cd_{0.2}Te$.

samples. Moreover, in previous works was not shown such drastic difference between the phonon spectra of the *n*- and *p*- $Hg_{0.8}Cd_{0.2}Te$.

The composition frequency dependencies for all observed phonon modes in p-type MCT-system at the temperature of 300K is presented on Figure 10. It is seen that these dependencies are similar to that one obtained in (Kozyrev et al., 1998) but the APMs observed in the spectral region 104 – 116 cm^{-1} are presented here also (are absented in work

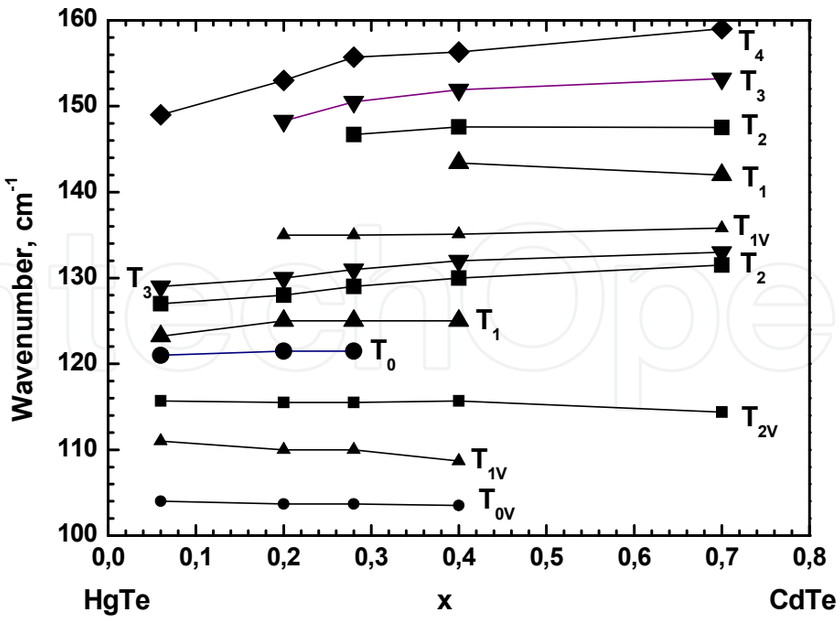

Fig. 10. The composition dependencies of the phonon mode frequencies for *p-*$Hg_{1-x}Cd_x$ *Te,* at temperature 300K.

of these authors). The amplitudes of these lines decrease with increasing of the CdTe-contain. That are the same lines which temperature behavior were described above for the *n*- and *p*-type $Hg_{0.8}Cd_{0.2}Te$. It is undoubtedly that these lines are related to the *HgTe*-pairs oscillations. It is possible to state that the APMs reproduce the CPM of HgTe-like band but are shifted to lower frequencies.

3.2 The random V-B model for ternary alloys

To understand and interpret the experimental data on the phonon spectra of the solid solutions it is necessary to describe mathematically the non-regular distribution of atoms in its lattices. It occurs that such description is possible in case of the strongly chaotically (stochastically) homogenous distribution what require a very great number of atoms and a very carefully mixed alloys. These conditions are fulfilled generally in case of the high quality homogenous semiconductor solid solutions of the III-V and II-VI semiconductor compounds. In this case we can use the Bernoulli equation (Ziman, 1979) describing a probability to occur a one from *n* equivalent events what can be apply to the probability to find one from *n* configurations in the solid solution lattice.

The crystalline structure of the most III-V and II-VI compounds (possessed zinc-blend or wurzit structure as was mentioned above) is characterized by basic cell – tetrahedron – each with a central ion surrounded in the first coordination shell by four nearest neighbours (NN) at the vertices. In a $A_xB_{1-x}Z$ ternary solid solution with substitution of the cation B by cation A, different tetrahedron configurations T_n (n is the number of B-atoms in the tetrahedron) coexist simultaneously: 2 strictly-binary ones corresponding to the AZ and the BZ compounds, whose lattices are characterized by the tedrahedron units T_0 and T_4 (configurations), respectively and 3 strictly-ternary ones actually characterized by the configurations T_1, T_2 and T_3. The similar configurations exist in a AY_xZ_{1-x} solid solution

where anions Z are substituted by anions Y – the tetrahedra will be looked at similarly because in zinc-blend lattice we can represent a basic unit as tetrahedron in two versions: centred by anion and surrounded by four cations or oppositely: four anions surround cation in centre.

The probability to find the T_n configuration in ideal lattice of the $A_xB_{1-x}Z$ or $AY_{1-y}Z_y$ ternary solid solution can be calculated using the Bernoulli polynomial (Ziman, 1979):

$$P_n(x) = \binom{4}{n}(1-x)^{4-n}x^n \tag{2}$$

where $\binom{4}{n} = \frac{4!}{n!(4-n)!}$ is the number of combinations with n elements in the fourth set:

$\binom{4}{0} = \binom{4}{4} = 1$, $\binom{4}{1} = \binom{4}{3} = 4$, $\binom{4}{2} = 6$, x is a mol composition of BZ compound in the solid solution what is equal to the ratio of the B-Z ion pairs per whole number of ion pairs in lattice.

It is obvious that probability $P_n(x)$ must be function of composition x because increasing of x means increasing of the B-atoms number in lattice what leads to increasing of the tetrahedron's number with high value of n (not higher then 4). The sum of probabilities to find all configurations in lattice of alloy with composition x must be equal to 1:

$$\sum_n^4 P_n(x) = 1 \tag{3}$$

The probabilities to find a some of cation A or B *in tetrahedron* T_n *in lattice* respectively are:

$$P_n^A(x) = \frac{4-n}{4}\binom{4}{n}(1-x)^{4-n}x^n \tag{4}$$

$$P_n^B(x) = \frac{n}{4}\binom{4}{n}(1-x)^{4-n}x^n \tag{5}$$

The same equations there are for the probabilities to find the certain of anions Z or Y respectively in the alloys $AY_{1-y}Z_y$:

$$P_n^Z(y) = \frac{n}{4}\binom{4}{n}(1-y)^{4-n}y^n \tag{4'}$$

$$P_n^Y(y) = \frac{4-n}{4}\binom{4}{n}(1-y)^{4-n}y^n \tag{5'}$$

It is easy to determine that

$$\sum_{n}^{4} P_n^A(x) = 1 - x \tag{6}$$

$$\sum_{n}^{4} P_n^B(x) = x \tag{7}$$

The same one takes place for the $AY_{1-y}Z_y$ alloys:

$$\sum_{n}^{4} P_n^Z(y) = 1 - y \tag{6'}$$

$$\sum_{n}^{4} P_n^Y(y) = y \tag{7'}$$

It is necessary to note that (4) and (5) are simultaneously the probabilities to find in the solid solution lattice the ion pairs *A*-*Z* and *B*-*Z*, respectively (in case of the $AY_{1-y}Z_y$ alloys, the probabilities to find the ion pairs *A*-*Z* and *A*-*Y* according Eqns. (4') and (5'), respectively).

The oscillator strength of the vibrational mode generated by a *A*-*Z*-dipole in the T_n configuration is (Robouch et al., 2001):

$$S_n^{A-Z}(x) = f_{AZ} N_0 P_n^A(x) \tag{8}$$

where f_{AZ} is the oscillator strength of the single dipole *A*-*Z*-pair, N_0 is total number of dipole pairs in the solid solution crystal, probability $P_n^A(x)$ is determined by (4).

It is important to remember that three assumption are introduced in this consideration:

1. the role of defects is negligible;
2. the alloy lattice is ideally homogenous and a random distribution of atoms in lattice takes place (stochastic homogeneity);
3. the oscillator strengths of the single dipole pairs for different configurations T_n are the same e.g. f_{AZ} or f_{BZ} depends not on index *n*.

If these conditions are fulfilled, the oscillator sum rule

$$\sum_n S_n^{A-Z}(x) = \sum_n f_{AZ} N_0 P_n^A(x) = f_{AZ} N_0 \sum_n P_n^A(x) = f_{AZ} N_0 (1 - x) \tag{9}$$

has to be satisfied.

Similarly for *B*-*Z* dipole pairs:

$$S_n^{B-Z}(x) = f_{BZ} N_0 P_n^B(x) \tag{10}$$

and the oscillator sum rule

$$\sum_n S_n^{B-Z}(x) = \sum_n f_{BZ} N_0 P_n^B(x) = f_{AZ} N_0 \sum_n P_n^B(x) = f_{BZ} N_0 x \tag{11}$$

In case of the $AY_{1-y}Z_y$ alloys the similar oscillator strengths sums must be fulfilled:

$$\sum_n S_n^{A-Z}(y) = f_{AZ} N_0 y \tag{10'}$$

$$\sum_n S_n^{A-Y}(y) = f_{AY} N_0 (1-y) \tag{11'}$$

Therefore, within this approximation the experimental Im ε(ω)-curves (obtained by Kramers-Kroning transformation from experimentally measured $R(\omega)$-curve) enable us to find the S_i values, to identify that with certain S_n^{A-Z} or S_n^{B-Z} and to verify the sums (10) or (11) what means the proportionality of the oscillator sum to the contain of the each component in alloy (N_0x is equal to molar percent of the BZ component and $N_0(1-x)$ – to the molar percent of the component AZ).

Some deviations of experimental data from the dependences (10) or (11) indicate evidently on considerable role of defects or others structural factors (non-random distribution).

3.3 Identification of observed lines in case of the n-$Hg_{0.2}Cd_{0.8}Te$ alloys

The probability to find the atoms Hg and Cd in the particular tetrahedra T_n (n is number of the Cd-atoms in tetrahedral) in the $Hg_{0.8}Cd_{0.2}Te$ lattice should be taken into account using formulas (4) and (5). If x=0.2 the values of $P_n^{Hg}(x)$ for different n are equal to: 0.410 (n=4), 0.307(n=2), 0.077(n=3) and 0.006(n=4) while the $P_n^{Cd}(x)$ values are: 0.102(n=1), 0.077(n=2), 0.192(n=3) and 0.002(n=4). At T=30 K all HgTe-like CPMs oscillate at the same frequency because tetrahedra with different number n are not deformed and we observed a degeneration of vibrational modes (Hg-Te and Cd-Te bonds have the same length). If T=300 K the splitting of the mode frequency takes place (see Fig.9): the most strong line at 122.6 cm^{-1} should be generate by Hg-Te dipoles in the T_0 tetrahedron while the line at 125.0 cm^{-1} – by this dipoles in the T_1 one and very small line at 128.6 – in the T_2. So, the frequency consequence takes place for HgTe-like modes: ${}^{HgTe}\omega_0 < {}^{HgTe}\omega_1 < {}^{HgTe}\omega_2 < {}^{HgTe}\omega_3$ according with work (Kozyrev et al., 1998). Analogical analyses for CdTe-like modes shown that the line at 151.5 cm^{-1} is generated by Cd-Te dipoles in T_1 tetrahedron and the line at 147.3 cm^{-1} – by the same dipoles in T_2 one. The frequency consequence for CdTe-like modes is: ${}^{CdTe}\omega_1 > {}^{CdTe}\omega_2 > {}^{CdTe}\omega_3 > {}^{CdTe}\omega_4$ what agree with the data of work (Kozyrev et al., 1998) also. It allow to find to what basic cells (tetrahedra) belongs each observed vibrational mode generating by Hg-Te and Cd-Te dipoles: corresponding tetrahedra are shown in Fig. 9 for CPM (T_n) as well as for APM (T_{nv}).

3.4 Identification of observed lines in case of the p-$Hg_{0.2}Cd_{0.8}Te$ alloys

The dissipation of the $Im[\varepsilon(\omega,T)]$ -curves on the Lorentzians was carried out for the p-type $Hg_{0.8}Cd_{0.2}Te$ sample (see Fig. 6). The parameters of these oscillators are presented in Tables 2 and 3. There are eight well-resolved oscillators for p-type $Hg_{0.8}Cd_{0.2}Te$ at 30 K and eleven for this sample at 300 K. The temperature dependencies of the phonon mode frequencies for p-$Hg_{0.8}Cd_{0.2}Te$ are presented in Fig. 8. We can see a considerably larger number of lines here in comparison with n-type sample but the temperature shift of the phonon mode frequencies is similar. Analogically was fined for what basic cells (tetrahedra) belongs each observed

vibrational mode generating by Hg-Te and Cd-Te dipoles: corresponding tetrahedra are shown in Fig. 8 for CPM (T_n) as well as for APM (T_{nv}).

3.5 Additional phonon modes

There are important guiding principles that the lines in the region 104 cm^{-1}- 116 cm^{-1} are related to the *Hg*-vacancies (Cebulski et al., 2008). This hypothesis can be verified by temperature dependences of the specific oscillator strength sum (SOSS) of the lines observed in this region. These temperature dependences are presented in Fig. 11 for *n*-$Hg_{0.8}Cd_{0.2}Te$ *Te* and Fig. 12 for *p*- $Hg_{0.8}Cd_{0.2}Te$. It is shown in Fig.11 that temperature dependencies of the SOSS of APM for *p*–type $Hg_{0.8}Cd_{0.2}Te$, have the exponential character described by function

$$\sum s_{HgTe}^{add} = 0.5 + 12\exp(-0.075 / kT) \tag{12}$$

with activation energy equal to 75 meV. It is too small energy in comparison with the Hg-vacancy activation energy to be equal to about 1eV (Chandra et al., 2003).

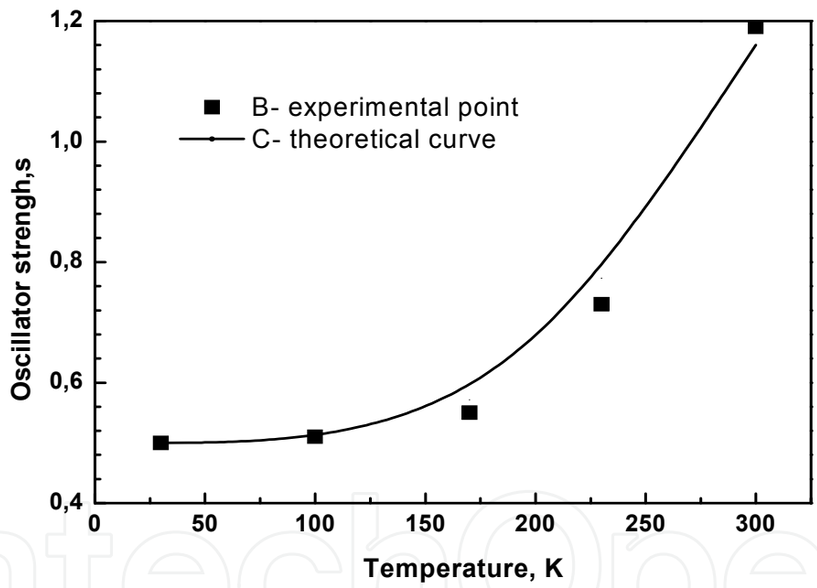

Fig. 11. The temperature dependence of the sum of the additional modes oscillator strengths for the *p*–type $Hg_{0.8}Cd_{0.2}Te$, B- experimental points, C is approximated curve calculated according the Equation
s=0,5+12exp(-0,075/kT).

The Fig.12 presents the temperature dependence of the SOSS of the same lines for *n*–type $Hg_{0.8}Cd_{0.2}Te$. This dependence is described by exponential function similar to (12):

$$\sum s_{HgTe}^{add} = 0.04 + 12\exp(-0.09 / kT) \tag{13}$$

with activation energy equal to 90 meV, which is larger than for p-type but is too small to be an activation energy for Hg-vacancies.

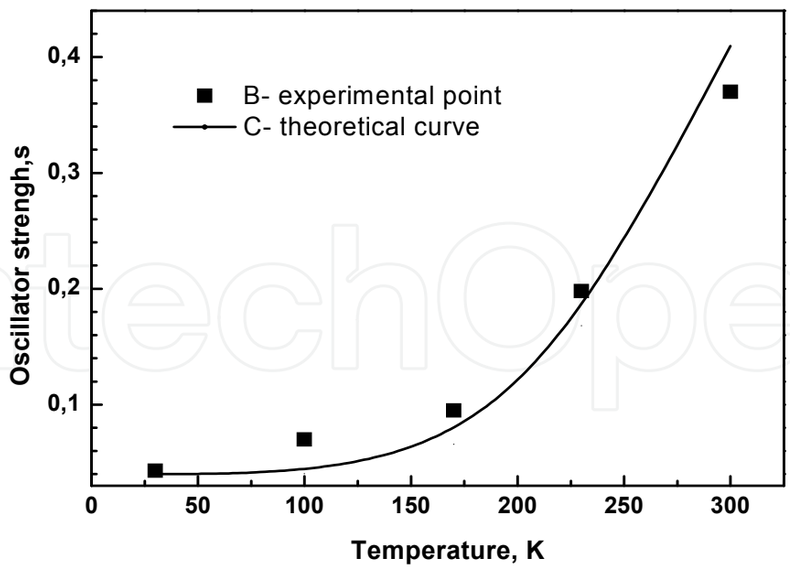

Fig. 12. The temperature dependence of the sum of the additional modes oscillator strengths for the *n* –type $Hg_{0.8}Cd_{0.2}Te$, B- experimental points, C is approximated curve calculated according the Equation
s=0,04+12exp(-0,09/kT).

It is clear that the temperature dependencies of the oscillator strength sum of the lines observed in the region of the 104 – 116 cm^{-1}, presented here, do not confirm the hypothesis that these lines are related to the *Hg*-vacancies. There are others doubtful circumvents, namely: in case of *n*-type $Hg_{0.8}Cd_{0.2}Te$ the single very weak line at 107 cm^{-1} is observed at 30 K also.

If we assume that this line is caused by Hg- vacancies it is necessary to agree that the vacancy density must be not less than 10^{18} cm^{-3}. While the data of the positron annihilation for *n*-type *HgCdTe* shown values of the *Hg*-vacancy concentration closer to 10^{15} cm^{-3} (Krause et al., 1990). It is necessary to note that method of the positron annihilation, seems to be direct method of the vacancy concentration measurement, in case of HgCdTe use the data of Hall-effect (in determination of the specific positron trapping rate) identifying the hole concentration to the concentration of Hg-vacancies. It is not completely correct because in *HgCdTe* there is always background of the electrically native compensated *Hg*-vacancies and real level of the Hg-vacancies is naturally higher than the hole concentration. Nevertheless, the Hg-vacancy density over 10^{18} cm^{-3} in the *n*- $Hg_{0.8}Cd_{0.2}Te$ *Te* of high quality (very high electron mobility of $2.5x10^5$ V/ms) is absolutely impossible.

The temperature dependences of the SOSS for discussed lines lead to the activation energy of process to be equal to 75 – 90 meV what could be as substantial argument for the model of two potential wells (Hg-atoms in lattice of HgCdTe) applying by *J.A. Sussman* (Sussman, 1967).

3.6 Two valley potential model and quasi quaternary alloys

J.A. Sussman (Sussman, 1967) proposed this model for the binary compounds. From this theory arise that a cation in the crystal lattice could have the two positions: first stable

position energetically more deep, second one is metastable state with higher energy and suitably with more long bond. This model related to HgTe and HgCdTe means that the Hg atoms can be shifted from the vertex position in tetrahedra (stable position) to a non centered position (metastable position). According to Sussman's theory such transition from stable to metastable state, means that the Hg-Te bonds become longer. The probability for such transition is described by

$$W = w \exp(-\Delta E / \kappa T) \tag{14}$$

where ΔE is the energy difference between the two states – stable and metastable one and w is the assumed probability at the absolute zero.

The temperature dependences of *SOSS* for APM shown in Figures 11 and 12 and described by relations (12) and (13) enable us to determine the ΔE. Therefore, in the case of *p*-type $Hg_{0.8}Cd_{0.2}Te$ the energy transition from the stable position of the *Hg* atoms to the metastable position is 75 meV and 90 meV for the n-type one. This difference can be explained by the fact that for *p*-type material where the considerable path of the crystal lattice is non relaxed, the density of metastable states is large than in *n*-type what could change the deep of the energy minimum (value E_2) for stable position. The ratio of the *SOSSs* of additional lines (104 -116 cm^{-1}) for *p*- and *n*-type materials is about one order. Therefore, the density of the metastable states and stable ones should differ with the same value. Simultaneously, the length of the *Hg-Te* bonds is longer for the metastable states in comparison with stable one. This difference have been appeared in *X*-ray analyses (Polit et al., 2010): 6.4604 Å for *n*-$Hg_{0.8}Cd_{0.2}Te$ and 6.4648 Å for *p*- $Hg_{0.8}Cd_{0.2}Te$ - the density of metastable states is larger of one order in *p*-type material and that causes statistically more long bonds Hg-Te.

3.7 General description of the HgCdTe phonon spectra

The general description of the phonon spectra is based on three Figures: 4, 5 and 6. These Figures present the temperature dependences of the HgTe-like and CdTe-like mode frequencies for *n*- and *p*-type $Hg_{0.8}Cd_{0.2}Te$ (Fig. 4 and 5) as well as the composition dependences of the same modes at the room temperature (Fig. 6). If temperature increases, the number of Hg-atoms occupied the meta-stable positions (Hg^{II}) increases also and the deformation of crystal lattice rises, respectively. The last factor can cause the removing of degeneracy of the HgTe-like CPMs in n-$Hg_{0,8}Cd_{0,2}\ Te$ when the temperature increases over the 100 K (see Fig. 5): the AVMs appear simultaneously, too. Indeed, the AVM at 112 cm^{-1} (beside very weak from 30 K at 108 cm^{-1}) take place after 100 K in n-type $Hg_{0.8}Cd_{0.2}Te$ and after 200 K appear additionally one AVM at 115-116 cm^{-1}. The presence of Hg^{II} in a tetrahedron leads to the stretching of bonds which in its turn causes the shift of the *Hg-Te* oscillation frequency towards smaller frequencies. This effect can occur in three kinds of tetrahedra: 1) containing *3 Hg*-atoms in stable position (Hg^{I}) and one Hg^{II} ; 2) containing two Hg^{I}, one Cd-atom and one Hg^{II}; 3) containing one Hg^{I}, two *Cd*-atoms and one Hg^{II}. The frequencies of *Hg-Te* oscillations in these tetrahedra should be arranged in the next sequence: the lowest frequency corresponds to the *Hg-Te* oscillations in the tetrahedron of first type and most higher corresponds to the oscillations in the tetrahedron of third type.

The lines in the range of 135 -137cm^{-1} are generated as could be assumed, by the oscillation of *Cd -Te* pair in the tetrahedra containing two Hg^{I}, one *Cd*-atom and one Hg^{II}. Therefore, the Figures 9,10 and 11 enable us to assume that the phonon spectra in *MCT* are reproduced in

two versions: first one is realized in the lattice consisted only from the Hg^{I}-atoms (that are *CPM*) and second one occurs in the lattice included the Hg^{II}-atoms too (that are *APM*). The theory of the quasi-quaternary alloys contained the two kind of *Hg* –atom position developed in (Cebulski et al., 2008) enable us to determine the Hg^{II} concentration on base of phonon spectra. The details of such consideration will be presented in next sub-chapter. As arise from this consideration, the sum of the specific oscillator strengths of *AVM* observed in the range 104 – 116 cm^{-1} is equal to

$$S^{Hg^{II}Te}_{(n-1),Hg^{II}}(y) = f_{HgTe}y \tag{15}$$

This simple expression enable us to determine experimentally (using the phonon spectra according to the the Eqn. (10)) the y – molar part of the Hg^{II}-atoms, assuming that: i) the lines corresponding to the *AVM* generating by tetrahedra bearing by Hg^{II} are identified correctly, ii) the specific oscillator strength of the Hg^{II} -Te oscillations in tetrahedra with Hg^{II}-atoms are the same as in tetrahedra without Hg^{II} atoms as was mentioned above. We assume that these conditions are fulfill in case of measured materials of *n*- and *p*-type $Hg_{0.8}Cd_{0.2}Te$. The calculated values of the molar fraction y of the Hg^{II}-Te obtained from phonon spectra (sum of the specific oscillator strength) are presented in Table IV for 30 *K* and 300 *K*.

Material	Sum of the specific oscillator strength for AVM		y, mol. %	
	30 *K*	300 *K*	30 *K*	300 *K*
n-type $Hg_{0.8}Cd_{0.2}Te$	< 0.043	0.37	< 0.7	6.3
p-type $Hg_{0.8}Cd_{0.2}Te$	0.50	1.1987	9.7	20.67

Table 4. Molar fraction of the Hg^{II} -atoms determine from phonon spectra

Reassuming we can affirm that in case HgCdTe of the *p*-type it consists of two sublattices: one sublattice contains the atoms of mercury in the stable state with the shorter length bonds of HgTe, second sublattice contains atoms Hg in the metastable state with the longer bond of HgTe. The phonon spectra of HgTe-like modes are reproduced for each above mentioned sublattices. Increase of the temperature leads to the increase of the number of Hg^{II} atoms (metastable state) and the same to the enlargement of tensions in the lattice what leads to splitting HgTe-like mod CPM in the n-type the material. Because of that differences between phonon spectra of n and p type in the room temperature are disappeared.

One can also affirm, that in the temperature 30K in the material n-$Cd_{0.2}$ $Hg_{0.8}Te$ is observed one HgTe-like mode and two CdTe - like of the mode (CPM) would confirm the percolation model of authors (Pages et al., 2009). It indicates (non directly) that the bond percolation thresholds x_c for the HgCdTe alloys is larger then 0.19, namely $x_c \geq 0.2$. Nevertheless, generally the V-B model developed for random case is confirmed completely for the HgCdTe solid solutions.

In Fig. 13 are shown the values of the oscillator strengths sums (OSS) for the Hg-Te dipoles and for Cd-Te dipoles for each samples investigated. The data are presented in two way: i) only OSS for CPMs are included (open circles and squares), for x=0.2 there are two open circles because first one (upper open circle) is regarded to *n-*$Cd_{0.2}$ $Hg_{0.8}Te$ and lower open circle – to *p-*$Cd_{0.2}$ $Hg_{0.8}Te$; ii) in the OSS are included the APM OSS also (filled circles and squares). That enable us to obtain the dependencies of the OSS on composition. As follow from Fig. 13 if the oscillator strengths of APM are included in the sum of the oscillator strengths for the modes generated by Hg-Te dipoles as well as Cd-Te dipoles the OSS are proportional to the contain of correspond compound: to the *x* in case of Cd-Te dipoles and to the *1-x* in case of Hg-Te ones. As was mentioned above (see Eqns. (9) and (11)) these dependences are considered as a criterion of applying the random V-B model to the phonon spectra interpretation of the ternary solid solutions. Therefore, the random version of the V-B model satisfactorily explains the high resolution FIR-spectra of ternary HgCdTe solid solutions if APM are included into consideration.

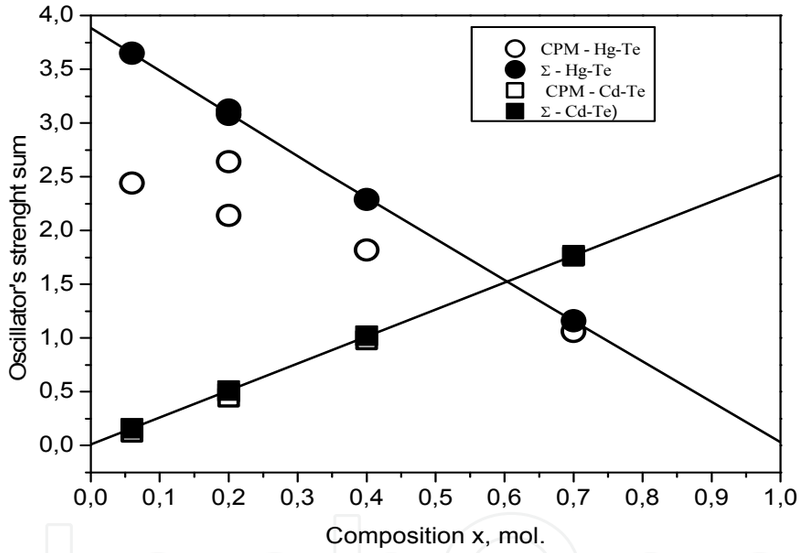

Fig. 13. The oscillator strength sum dependence on composition for the HgCdTe alloys

3.8 Spectral analyses of the FIR-spectra for quaternary alloys

The Kramers – Kronig analysis was applied to determine the position of observed lines. In Fig. 14 and 15 are shown the curves of imaginary part of dielectric function Im $\varepsilon(\omega,x,y)$ for compositions VI and VII (see Table 1) respectively, obtained by Kramers-Kroning transformation from the reflectivity curves presented in Fig. 4 and 5 at 30 K. The imaginary part of dielectric function for $Zn_xCd_yHg_{(1-x-y)}Te$ solid solution can be presented as the superposition of Lorentzians as it is follow from Eqn. (1). The fittings by the Lorentzian sums are presented in Fig.14 and 15 too. The parameters of Lorentzians are presented in Tab. 5 and 6 respectively.

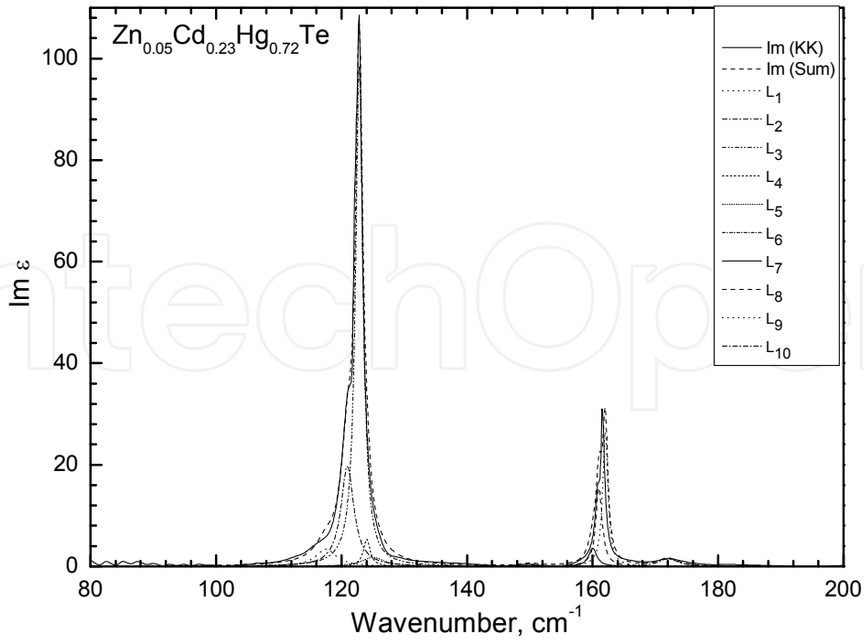

Fig. 14. Spectral analysis for Sample $Zn_{0,05}Cd_{0,23}Hg_{0,72}Te$ (sample VI).

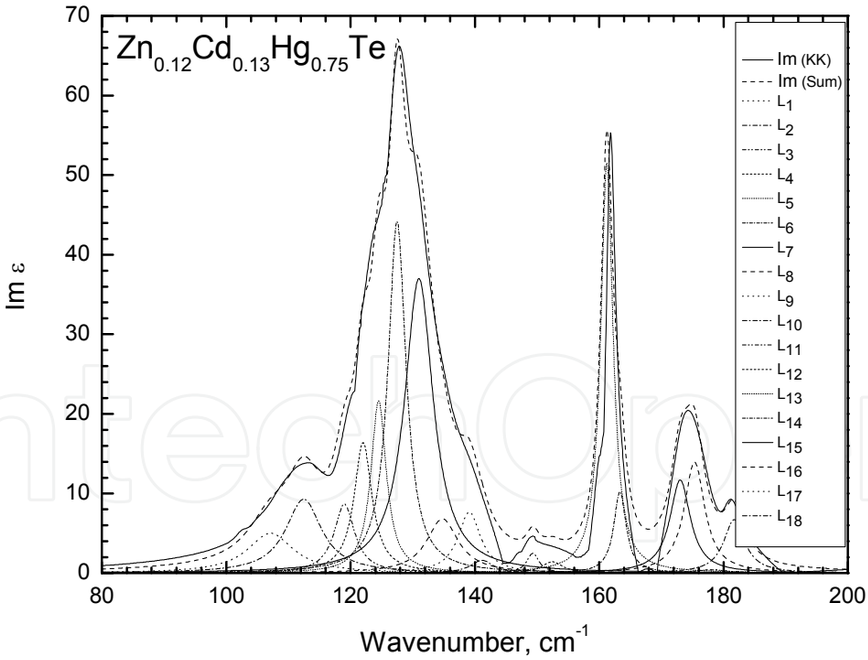

Fig. 15. Spectral analysis for sample $Zn_{0,12}Cd_{0,13}Hg_{0,75}Te$ (sample VII).

The present analysis shows that the investigated quaternary ZMCT has lager number of the resonance frequencies in the observed spectra compared to the ternary solid solutions of the binary HgTe, CdTe and ZnTe (118 to 180 cm^{-1}) and extends the frequency region of the phonon modes – from 108 to 190 cm^{-1}.

Frequency (cm^{-1})	Oscilator strength (cm^{-2})	Damping factor (cm^{-1})
107,20	4847	9,02
112,50	7341	7,02
119,00	4130	4,00
122,00	7000	3,50
124,50	8090	3,00
127,47	19700	3,50
131,00	27000	5,57
134,80	5700	6,20
139,10	4700	4,40
141,10	1000	4,40
149,30	900	2,40
152,40	890	4,10
160,20	4410	2,40
163,30	4000	2,40
173,00	8100	4,00
175,30	9800	4,00
178,00	483	6,40
181,70	5000	4,10

Table 5. Parameters of Lorentzians presented in Fig.10 for sample VII

Frequency (cm^{-1})	Oscilator strength (cm^{-2})	Damping factor (cm^{-1})
117,52	1600	4,02
120,92	6000	2,52
122,80	17041	1,41
124,00	860	1,30
125,00	1000	4,50
150,00	200	3,00
160,00	900	1,57
161,00	3000	1,20
162,00	4300	1,00
172,00	1000	3,80

Table 6. Parameters of Lorentzians presented in Fig.9 for sample VI.

It is necessary to use 10 oscillators to fit the Im $\varepsilon(\omega,x,y)$ curve (x=0.05, y=0.23) – sample VI, and 18 ones to fit the Im $\varepsilon(\omega,x,y)$ curve (x=0.12, y=0.13) – sample VII. The identification of observed lines in obtained spectra will be performed in the frame of the V-B model developed for random distribution of atoms in the lattice for quaternary solid solutions.

3.9 The random V-B model for quaternary alloys

We consider here the four-component solid solution $A_xB_y\,C_{1-x-y}Z$ with three kinds of cations *A*, *B* and *C* and with the same anion *Z*. The lattice of quaternary alloy contents 15 basic units (tetrahedra): three binary *AZ*, *BZ*, *CZ*, nine strictly ternary *ABZ*, *ACZ*, *BCZ* and three strictly quaternary *ABCZ*. If quaternary alloy have *x* mol part of *AZ* compound and *y* mol part of *BZ* we can determine the probability to find in lattice the tetrahedron T_{nm} with *n* A-cations and *m* B-cations. This probability is equal to:

$$P_{n,m}(x,y)=\binom{4-n}{m}\binom{4}{n}(1-x-y)^{4-n-m}x^n y^m \tag{16}$$

where matrixes $\binom{4-n}{m}$ and $\binom{4}{n}$ are the same number of combinations as in Eqn. (2).

It is seen that if y=0 and m=0, the Eqn.(16) is:

$$P_n(x)=1\cdot\binom{4}{n}(1-x)^{4-m}\cdot x^n\cdot 1 \tag{17}$$

and the Eqn. (2) takes place for an alloy $A_xC_{1-x}Z$.

At least, it is possible to consider when *1-x-y* = 0, *4-n-m* = 0. In this case *y* = *1-x* and *m* = *4-n*, therefore

$$P_{n,m}(x,y)=\binom{4-n}{m}\binom{4}{n}\cdot 1\cdot x^n\cdot y^m \tag{18}$$

and we obtain the probability to find a tetrahedron T_n for an alloy A_xB_yZ. It means that Eqn. (16) really correctly described the random distribution of atoms in the quaternary solid solutions $A_xB_y\,C_{1-x-y}Z$. The correspond probabilities to find particular cations in tetrahedron $T_{n,m}$ in lattice are:

$$P_n^A(x)=\frac{n}{4}\binom{4-n}{m}\binom{4}{n}x^n y^m(1-x)^{4-n-m}, \tag{19}$$

for cation *A*;

$$P_n^B(x)=\frac{m}{4}\binom{4-n}{m}\binom{4}{n}x^n y^m(1-x)^{4-n-m}, \tag{20}$$

for cation *B*, and

$$P_n^C(x) = \frac{4-n-m}{4}\binom{4-n}{m}\binom{4}{n}x^n y^m (1-x)^{4-n-m} \tag{21}$$

for cation *C*.

By this way the Eqns. (2, 4, 5, 16, 19 – 21) represent the complete description of the random atom distribution in the ternary $A_xB_{1-x}Z$ and quaternary $A_xB_y\ C_{\ 1-x-y}Z$ solid solutions with substitution of cations. The four-component solid solution $A_xB_yC_{\ 1-x-y}Z$ in ideally random case described by relations (16) and (19-21) consists from fifteen structural units – tetrahedra – which can generate 66 optically active phonon (vibrational) modes. These number of modes arose by next way: three strictly binary tetrahedra generate three vibrational modes AZ-like, BZ-like and CZ-like, nine (3x3) strictly ternary tetrahedra generate 9x6=54 vibrational modes and three strictly quaternary tetrahedra generate 3x3=9 vibrational modes: in sum 66 vibrational modes. In practice the most of these modes are degenerated (have the same frequencies): for example, the AZ-like modes generated in tetrahedra ABZ could have the same frequencies as AZ-like modes in tetrahedra ACZ. The same concerns the BZ-like and CZ-like modes. By this way the number of distinguished modes should be 30.

The expression for the oscillator strengths are similar as for ternary alloys:

$$S_{n,m}^{A-Z}(x,y) = f_{AZ}N_0P_{n,m}^A(x,y) \tag{22}$$

where probability $P_{n,m}^A(x,y)$ is determined by (19). Similarly are given the expression for $S_{n,m}^{B-Z}$ and $S_{n,m}^{C-Z}$. The corresponding oscillator sum rule are:

$$\sum S_{n,m}^{A-Z} = N_0 f_{AZ}(1-x-y) \tag{23}$$

$$\sum S_{n,m}^{B-Z} = N_0 f_{BZ}x \tag{24}$$

$$\sum S_{n,m}^{C-Z} = N_0 f_{CZ}y \tag{25}$$

The role of these oscillator sum rules would be the same as in ternary alloys but in the practice it is more difficult to relies the verification of the random distribution of atoms because the number of theoretically possible modes is very large and this factor prevent calculation of the oscillator sum rule.

3.10 Identification of observed lines in case of the $Zn_xCd_yHg_{1-x-y}Te$ alloys

An oscillator strength of particular mode enables us to determine the fraction of basic tetrahedral cells and interpret observed lines in phonon spectra. The attempt to interpret the spectra for sample VI (Fig. 9) and sample VII (Fig.10) is presented in Table 7. Here are presented results of the probabilities to find one of three dipole pairs (Hg-Te, Cd-Te, Zn-Te) in corresponding tetrahedron in lattice calculated according Eqn. (19-21) practically for all possibilities configurations in lattice of the $Zn_xCd_yHg_{1-x-y}Te$ alloys. There are observed modes generated by dipoles in cells probabilities to find of which in lattice is not less than 0.02. Summarizing the above mentioned results on the quaternary $A_{1-x-y}B_xC_yZ$ alloys, it is

Tethraedra	Dipole-pairs	Probablities	Composition VI, n-type	Composition VII, p-type	Nr of line
$2Hg^{II}2Cd$ $1Zn\ 1Cd\ 2Hg^{II}$	Hg - Te	0,002 –0,007		**107,2 cm^{-1}**	1
$1Hg^{II}3Cd$ $1Zn\ 2Cd\ 1Hg^{II}$	Hg - Te	$8 \cdot 10^{-3}$- $2 \cdot 10^{-3}$		**112,5 cm^{-1}**	2
4 Hg	Hg - Te	0,37 - 0,24	**117,5 cm^{-1}**	**119.0 cm^{-1}**	3
1Zn 1Cd 2Hg	Hg - Te	0,06 – 0,01	**120,92 cm^{-1}**	**122,3 cm^{-1}**	4
2Hg 2Cd	Hg - Te	0,05 - $7 \cdot 10^{-4}$		**124,5 cm^{-1}**	5
3Hg 1Zn	Hg - Te	0,18 - $2 \cdot 10^{-2}$	**122,8 cm^{-1}**	**127,5 cm^{-1}**	6
3Hg 1Cd	Hg - Te	0,28 - 0,13	**124,0 cm^{-1}**	**131,0 cm^{-1}**	7
2Hg 2Zn	Hg - Te	0,05 - $7 \cdot 10^{-4}$	**125. 0 cm^{-1}**	**134,8 cm^{-1}**	8
1Zn 1Cd 1Hg	Hg - Te	0,07 - 0,02		**139,1 cm^{-1}**	9
1Hg 3Cd	Hg - Te	$6 \cdot 10^{-3}$ - $1,2 \cdot 10^{-3}$			
1Hg 3Zn $2Zn\ 1Cd\ 1Hg$	Hg - Te	$4 \cdot 10^{-3}$ - $6 \cdot 10^{-6}$			
4Cd	Cd - Te	0.02 - $2 \cdot 10^{-4}$		**141,1 cm^{-1}**	10
1Hg 3Cd	Cd - Te	0,02 - 0,004	**150,0 cm^{-1}**	**149,3 cm^{-1}**	11
2 Hg 2Cd	Cd - Te	0,07 - 0,02	**160 cm^{-1}**	**152,4 cm^{-1}**	12
1Zn 2Cd 1Hg	Cd - Te	0,015 – 0,004	**161,5 cm^{-1}**	**160,2 cm^{-1}**	13
3Hg 1Cd	Cd - Te	0,09 - 0,04			
3Hg 1Zn	Zn - Te	0,056 - $9 \cdot 10^{-3}$	**162,0 cm^{-1}**	**163,0 cm^{-1}**	14
1Zn 3Cd	Cd - Te	$1,9 \cdot 10^{-3}$ - $4,8 \cdot 10^{-4}$			
2Hg 2Zn	Zn - Te	0,05 - $7 \cdot 10^{-4}$			
2Zn 2Cd	Cd - Te	$1,4 \cdot 10^{-3}$ - $5 \cdot 10^{-5}$			
1Hg 3Zn	Zn - Te	$1,2 \cdot 10^{-2}$ - $1,9 \cdot 10^{-5}$			
3Zn 1Cd	Cd - Te	$7 \cdot 10^{-4}$ - $2 \cdot 10^{-6}$			
1Zn 1Cd 2Hg	Cd -Te	0,032 - 0,007			
1Zn 3Cd	Zn - Te	$1,6 \cdot 10^{-4}$ - $6,5 \cdot 10^{-4}$			
2Zn 1Cd 1Hg	Cd - Te	$8 \cdot 10^{-3}$ - $2 \cdot 10^{-4}$			

Tethraedra	Dipole-pairs	Probablities	Composition VI, n-type	Composition VII, p-type	Nr of line
2Zn 2Cd	Zn - Te	$5 \cdot 10^{-5}$ - $1{,}4 \cdot 10^{-3}$			
3Zn 1Cd	Zn - Te	$2 \cdot 10^{-3}$ - $5 \cdot 10^{-6}$			
1Zn 1Cd 2Hg	Zn - Te	0,032 - 0,007	**172,0 cm^{-1}**	**173,0 cm^{-1}**	15
2Zn 1Cd 1Hg	Zn - Te	0,02 - $4 \cdot 10^{-4}$		**175,3 cm^{-1}**	16
1Zn 2Cd 1Hg	Zn- Te	$7 \cdot 10^{-3}$ - $2 \cdot 10^{-3}$		**178,0 cm^{-1}**	17
4Zn	Zn - Te	$1 \cdot 10^{-3}$ - $2 \cdot 10^{-6}$		**181,7 cm^{-1}**	18

Table 7. Interpretation of observed lines in FIR spectra of $Zn_xCd_yHg_{1-x-y}$ Te

possible to conclude that 21 different modes are distinguished among the high resolution FIR-spectra of the seven composition of the ZnxCdyHg1-x-yTe alloys measured. By this way, the V-B random model developed for the quaternary alloys enable us to identify the observed structure of the sub-bands in the high resolution FIR-spectra ffor the ZnxCdyHg1-xyTe alloys.

The next step is calculation of the OSS for certain dipole pairs. It is reason to consider the dependence on composition of the OSS for Zn-Te dipoles (the ZnTe contain is changed from 0.05 to 0.18). In Table 8 are shown calculated OSS for this dipoles.

Number of sample	x, mol	OSS for Zn-Te
I	0.02	0.065
VI	0.05	0.197
II	0.07	0.211
VII	0.12	0.769
V	0.18	0.907

Table 8. The oscillator strength sum for Zn-Te dipoles in measured samples of $Zn_xCd_yHg_{1-x-y}Te$

From Table 8 follow that OSS for Zn-Te dipoles is really approximately proportional to contain of ZnTe (values of x) in the $Zn_xCd_yHg_{1-x-y}Te$ alloys. Therefore, this important consequence of the V-B random model (Eqn.25) is fulfilled for the semiconductor quaternary alloys also.

4. Conclusion

Those, the high resolution FIR-spectra of the ternary HgCdTe and quaternary HgZnCdTe alloys obtained by using of the synchrotron radiation as source enable us to decipher the tangled phonon spectra in these kinds of the semiconductor solid solutions applying the random version of the V-B model for its interpretation.

The results described above can give affirmative answer on the question: whether geometry of chaos e.g. the Bernoulli equation is enough to describe the oscillator strengths of observed lines in FIR-spectra if the Additional Phonon Modes will be involved in sums of the oscillator strengths.

Presented here cycle of researches dedicated to the ternary $Hg_{1-x}Cd_xTe$ cannot confirm but allow us to assume that the HgTe-like CPMs for $x \leq 0.2$ are extending and dispersion relation should be exist for them (as was shown the data on Magnetophonon Resonance confirm this assumption (Sheregii & Ugrin, 1992)).

5. References

Adachi Sadao, *Optical Properties of Crystalline Solids and Amorphous Semiconductors. Materials and Fundamental Principles*, Kluver Academic Publishers, Boston, 1999

Amirtharaj P.M., Dhart N.K, Baars J. and Seelewind H., *Semicond. Sci. Technol.* 5, S68 (1990)

Baars J. and Sorgers F., *Solid State Commun.*10, 875 (1972)

Barker A.S. and Sievers J., *Rev. Modern Phys.* 47, S1 (1975)

Biao Li.,.Chu J.H, Ye H.J., Guo S.P., Jiang W., Tang D.Y., *Appl.Phys.Lett.* 68, 3272 (1996)

Cebulski J., Ge˛bicki W., Ivanov-Omskii V.I., Polit J., Sheregii E.M., *J. Phys.: Cond. Matter* 10, 8587 (1998)

Cebulski J., Sheregii E. M., Polit J., Marcelli A., Piccinini M., Kisiel A., Kucherenko I., Triboulet R., *Appl. Phys. Lett.* 92, 121904 (2008)

Cestelli Guidi M., Piccinini M., Marcelli A., Nucara A., Calvani P., Burattini E., *Journal of the Optical Society of America*, A22, 2810 (2005)

Chandra D., Schaake H.F., Kinch M.A., *J. Electronics Materials*, 32, 810, (2003).

Kosevich A.M., *The crystal lattice,* WILEY-VCH, Berlin-NewYork, (1999)

Kozyrev S.P., L.K. Vodopyanov, R.Triboulet, *Phys. Rev. B,* 58, 3, 1374 (1998).

Krause R., Klimakow A., Kiessling F.M., Polity A., Gille P., Schenk M., *J. Cryst.Growth.*, 101, 512 (1990)

Marcelli A., Cesteli Guidi M., Piccinini M., Innocenzi P., Malfatti L., Xu W., *Phys. Stat. Sol.C*,6, 1999 (2009)

Pagès O., Souhabi J., Postnikov A. V., and Chafi A., *Phys. Rev. B* 80, 035204 (2009)

Polit J., E.M. Sheregii, J. Cebulski, A. Marcelli, B. Robouch, A. Kisiel, A. Mycielski, *Phys. Rev. B*, 82, 014306 (2010)

Rath S., Jain K.P., Abbi S.C., Julien C., Balkanski M., *Phys . Rev. B* ,52, 24, 17172 (1995)

Robouch B., Kisiel A. and Sheregii E. M., *Phys. Rev B.*, 64, 073204 (2001)

Sher A., Chen A.B., Spicer W.E. and Shih C.K., *J. Vac. Sci. Technol.* A3, 105 (1985)

Sheregii E. M. and Ugrin Yu. O., *Sol. State Comm.*, 83, 1043 (1992)

Sheregii E. M., J. Cebulski, A. Marcelli, M. Piccinini, *China J. Phys.*, 102, 045504 (2011)

Sheregii E.M., Cebulski J., Marcelli A. and Piccinini M., *Phys. Rev. Lett.* 102, 045504 (2009)

Sheregii E.M., J. Polit , J. Cebulski, A. Marcelli, M. Castelli Guidi, B. Robouch, P. Calvani, M. Piccinini,, A. Kisiel, I. V. Ivanov-Omskii, *Infrared Physics & Technology* 49, 13 (2006)

Sussmann J.A. ,*J.Phys.Solids* ,28,1643,(1967)

Talwar D.N., *J.Appl.Phys.* 56, 1601 (1984)

Taylor D.W. in: Elliot R.J., Ipatova I.P. (Eds), *Optical properties of mixed crystals*, Elsevier Science Publishers, Amsterdam, pp. 35-131, (1988)

Verleur H.W. and Barker A.S., *Phys. Rev.* 149,715 (1966).
Ziman J.M., *Models of disorder*, Cambridge University Press, Cambridge, England, 1979

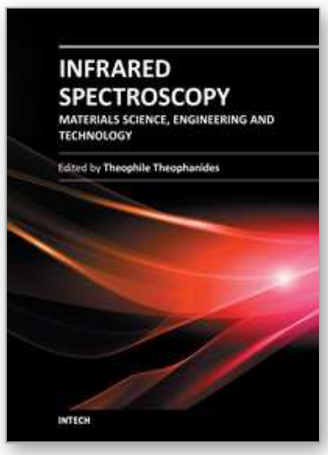

Infrared Spectroscopy - Materials Science, Engineering and Technology

Edited by Prof. Theophanides Theophile

ISBN 978-953-51-0537-4
Hard cover, 510 pages
Publisher InTech
Published online 25, April, 2012
Published in print edition April, 2012

The present book is a definitive review in the field of Infrared (IR) and Near Infrared (NIR) Spectroscopies, which are powerful, non invasive imaging techniques. This book brings together multidisciplinary chapters written by leading authorities in the area. The book provides a thorough overview of progress in the field of applications of IR and NIR spectroscopy in Materials Science, Engineering and Technology. Through a presentation of diverse applications, this book aims at bridging various disciplines and provides a platform for collaborations among scientists.

How to reference

In order to correctly reference this scholarly work, feel free to copy and paste the following:

E.M. Sheregii (2012). High Resolution Far Infrared Spectra of the Semiconductor Alloys Obtained Using the Synchrotron Radiation as Source, Infrared Spectroscopy - Materials Science, Engineering and Technology, Prof. Theophanides Theophile (Ed.), ISBN: 978-953-51-0537-4, InTech, Available from: http://www.intechopen.com/books/infrared-spectroscopy-materials-science-engineering-and-technology/high-resolution-spectra-of-semiconductor-s-alloys-obtained-using-the-far-infrared-synchrotron-radi

INTECH
open science | open minds

InTech Europe
University Campus STeP Ri
Slavka Krautzeka 83/A
51000 Rijeka, Croatia
Phone: +385 (51) 770 447
Fax: +385 (51) 686 166
www.intechopen.com

InTech China
Unit 405, Office Block, Hotel Equatorial Shanghai
No.65, Yan An Road (West), Shanghai, 200040, China
中国上海市延安西路65号上海国际贵都大饭店办公楼405单元
Phone: +86-21-62489820
Fax: +86-21-62489821

IntechOpen